A Three-Dimensional Transient Model for Evaluating the Performance of Cement-Based Thermoelectric Module

Xiaoli LIU[1], Ming QU[2]*, Kazuaki YAZAWA[3]

[1]Lyles School of Civil Engineering, Purdue University,
West Lafayette, IN 47907, U.S.A
liu2251@purdue.edu

[2]Lyles School of Civil Engineering, Purdue University,
West Lafayette, IN 47907, U.S.A
mqu@purdue.edu

[3]Birck Nanotechnology Center, Purdue University,
West Lafayette, IN 47907, U.S.A
kyazawa@purdue.edu

* Corresponding Author

ABSTRACT

The thermoelectric module (TEM) is a device that integrates multiple thermoelectric (TE) elements to realize the mutual conversion of heat and power. Due to the advantages of no moving parts and flexible expansion, the application of conventional Bi_2Te_3-based TEM in buildings has attracted the attention of researchers. On the other hand, the TE behavior of hardened cement composites was found by combining conductive additives with cement. Therefore, a new study on cement-based TEM for building energy harvesting and temperature control is proposed. To simulate the performance of cement-based TEM, a three-dimensional heat transfer model considering temperature-dependent TEM characteristics was established. The validity of the model is verified by comparing the results with commercial simulation software and experiments. Different from the existing analytical models and commercial software, the customized model has greater scalability, optimization, and control flexibility. Through parametric studies, the model can guide the design of TEM and the development of TE cement.

1. INTRODUCTION

The building sector currently accounts for over one-third of the continuously increasing global energy consumption and CO_2 emission (IEA (2020), n.d.). The severe energy and environmental issues cause extreme weather, which in turn leads to a vicious cycle of growing energy demand in buildings. Energy demand encourages the effort to develop high-performance and net-zero energy buildings that can take advantage of environmental changes as well as renewable and waste energy.

Thermoelectric technology is one of the promising routes to reduce energy consumption and adjust the built environment. TE materials realize the interconversion of thermal and electrical energy. Power can be generated from the TE material under a certain temperature difference, and the surface temperature difference can form for given power input to the same TE material. TE materials can be classified as *n-type* or *p*-type when electrons or holes dominate the charge transport, respectively. The *n-type* and *p*-type materials can be connected thermally in parallel and electrically in series. One *p-n* pair forms a TE couple and multiple TE couples constitute the TE module (TEM).

TEM works under cooling/heating mode is called TE cooler (TEC) or TE heat pump (TEH) while that under generation mode is named as TE generator (TEG).

The application of commercially available TEMs in building enclosure and energy systems keeps increasing over the last ten years (Zuazua-Ros et al., 2019). Potentially, TEM can work in four different modes in buildings. In the sunny summer, the maximum temperature of urban surfaces (i.e. wall, roof, pavement) may reach 55~70°C due to solar radiation, accelerating the urban heat island effect (Svobodová & Matějka, 2014). TEG can be used to absorb heat from the urban surface and transform it to free electricity, as a result, lowering the surface temperature (Figure 1a). In winter, there is also a temperature difference between indoors and outdoors, similarly, generating power in the opposite direction (Figure 1c). But to perform active heating or cooling, direct current (DC) with different directions can be applied to the system as shown in Figure 1b and 1d. This TE-building system has many merits such as no moving part, expansion flexibility, better thermal comfort, etc.

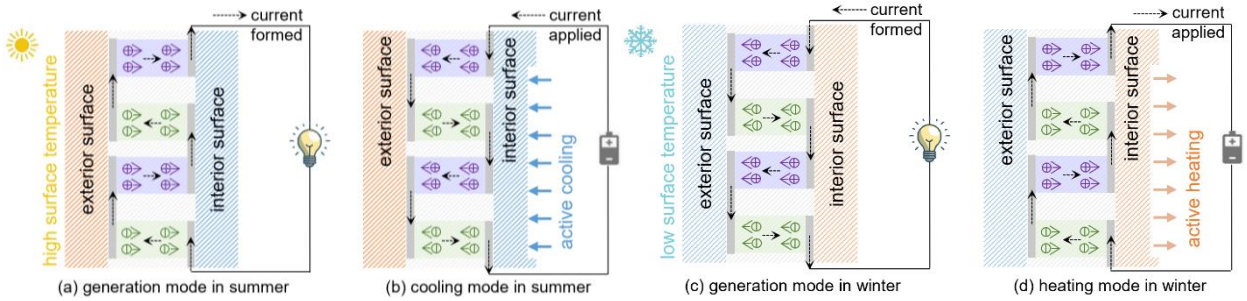

Figure 1: TE envelope working under different operating conditions: (a) generation mode in summer, (b) cooling mode in summer, (c) generation mode in winter, and (d) heating mode in winter

On the other hand, interesting finds of TE behaviors in hardened cement composites have been reported. These TE cement composites are produced by adding conductive additives (i.e. carbon fiber, graphite powder, metallic oxide power, etc.) to cement (Ghosh et al., 2019, 2020). Therefore, a research hypothesis was proposed to replace the commercial TEM with cement-based TEM for the design of a highly integrated system and the usage of environmentally friendly materials. However, the study on TE cement is still in the early stage. Very few papers reported the performance of the cement-based thermocouple and so far, no cement-based TEM was successfully manufactured. Thus, the model is of great significance to the performance prediction of the cement-based TEM.

The heat transfer model of TEM includes a simplified model, analytical model, and numerical model. The simplified model is mostly used in many system-level modelings (Liu et al., 2020). The model treats the whole TEM as a lumped system and analyzes the heat transfer at two boundary points (i.e, hot side and cold side) given the overall properties of TEM. The analytical model is assumed to have higher accuracy and computational speed as compared with the numerical model which executes a set number of iterations. But it is not easy to obtain analytical solutions to complex partial differential equations (PDEs) unless the model is simplified to lower dimension and ideal assumptions (i.e. no Thomson effect, no surface heat loss, constant properties, even distribution of charge density, etc.). The Numerical model can overcome this limitation and solve complex PDEs. In 2004, El-genk et al. presented a detailed algorithm of FEM for the 3D TEG model (El-Genk' et al., 2004). At the same time, Hogan and Shih summarized the modeling methods and governing PDEs for TE element (Hogan & Shih, 2005), then Antonova and Looman simulated the performance of a 2D TE leg in ANSYS, which helped the development of the TE package in commercial simulation software (Antonova & Looman, 2005). Later, customized numerical models were studied by finite difference method (FDM) and finite volume method (FVM), as shown in Table 1.

Table 1: Summary of customized numerical models of the thermoelectric module

Method	State	Material	Property	Error	Ref
FDM	1D Steady-state	Marlow DT12-6L	T-dependent	<5%	(Rodríguez et al., 2009)
	1D Steady-state	HMS + MgSi	T-dependent	~7.2%	(Fateh et al., 2014)
	1D Transient	commercial TEM	Constant	~20%	(Nguyen & Pochiraju, 2013)
	3D Steady-state	Bi_2Te_3	Constant	<8%	(Jang & Tsai, 2013)

FVM	1D steady-state	Bi_2Te_3	Constant	<1% (analytic) <6.6% (FEM) <27.4% (test)	(Pfeiffelmann et al., 2018)
	1D Transient	Bi_2Te_3	T-dependent	~5%	(Yan et al., 2014)
	2D steady-state	Bi_2Te_3	Constant	<10%	(Oliveira et al., 2014)

This research developed a 3D heat transfer model to simulate the performance of cement-based TEM by using the properties of TE cement in the literature, which is of significance for the TE cement development and application. The customized model solved via FVM can be designed to control the temperature-dependent characterizations, Thomson effect, surface heat loss, etc. Compared with many existing models built-in commercial simulation software, this model can be better integrated with building energy consumption simulation software, which can optimize the TEM geometry and add a control system. Therefore, the custom model has better extensibility, flexibility, optimization, and control performance. This paper first introduces the method of the TEM model, including governing equations, boundary conditions, and flow of the algorithm. Then, the accuracy of the model is verified by comparing it with the experimental results. In the simulation part, a parametric study is presented to analyze the impact of several factors and global optimization is carried out to guide the design of TEM.

2. NUMERICAL MODELING

2.1 Model Development

As shown in Figure 1, our model considers applications at varying ambient temperatures. In summer, the air convection and solar radiation heat the exterior surface to 60 ºC, while the indoor temperature is constant at 22 ºC. We explored how much power the TE generator can form given the temperature difference around 35 ºC. In addition, the effect of the TE cooler on the regulation of room temperature was also analyzed during the moderate season.

Therefore, a 3D heat transfer model was established for TEM to simulate and evaluate its performance in different proposed scenarios. The model considers temperature-dependent TE properties, the Thomson effect, and thermoelectric contact resistance. A 3D partial differential governing equation was established for the transient heat transfer process of a TE element, and the corresponding variation of the electric potential was modeled by Ohm's Law. The FVM was used to solve the PDE. Considering the symmetry of TEM, the overall heat transferred, and power generated by the module becomes a linear extension of all TE elements. The model was finally validated by the experimental results.

The assumptions we made for the model include that:

- The material properties are isotropic;
- The surface heat loss of the TE element is ignored;
- The charge is uniformly distributed, and the direction of current density is perpendicular to ceramic plates.

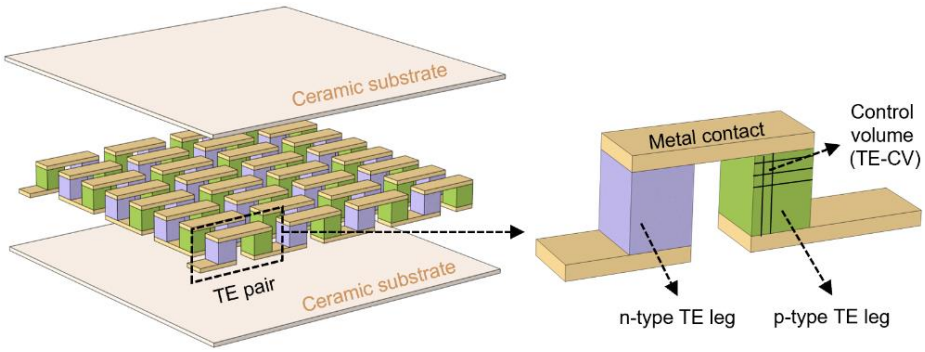

Figure 2: Schematic diagrams of a TE module and a TE couple.

The heat transfer mechanism in a TE material includes heat conduction, heat convection, radiation, Joule heat, Thomson effect, Peltier effect, Bridgeman effect, etc. as listed in Table 2 (Goupil, n.d.). The heat conduction occurs due to the temperature difference between two ends of the TE material, which follows Fourier's Law. The convective

and radiative heat transfer may exist between the surface of the TE material and the surroundings, known as heat losses. Joule heating comes from the carrier movement through a conductor, as calculated by Joule's first law. Different from Joule heating which affects the whole electric conductor, the Peltier effect transfers heat from one electrical junction to another. The volumetric heat source from the Peltier effect is calculated by $T\boldsymbol{J}_e(\nabla S)_T$. It shows that this term is related to the gradient of the Seebeck coefficient with respect to the position (x, y, z) when the temperature is constant. Hence, this term will not play a role once the Seebeck coefficient is isotropic. In this model, the Peltier source is considered as a boundary condition at two junctions of the TE material. The Bridgeman effect is caused by the non-uniform distribution of charge. Since we assume that the charge is uniformly distributed, this source term can also be ignored. The multidimensional heat equation follows the energy conservation in terms of temperature for the TE material, which is written in equation (1). The expressions of all volumetric heat sources in a TE material are also summarized in Table 2.

$$\dot{q}_{st} = \dot{q}_F + \dot{q}_J + \dot{q}_p + \dot{q}_T + \dot{q}_B + \dot{q}_{loss} \tag{1}$$

Table 2: Volumetric source terms

Fourier ($\dot{q}_F$)	**Joule ($\dot{q}_J$)**	**Peltier ($\dot{q}_P$)**	**Thomson ($\dot{q}_T$)**	**Bridgeman ($\dot{q}_B$)**	**Surface Loss ($\dot{q}_{loss}$)**
$\nabla(\kappa_{tot}\nabla T)$	$\boldsymbol{J}_e^2/\sigma$	$T\boldsymbol{J}_e(\nabla S)_T$	$-\tau\boldsymbol{J}_e \cdot \nabla T$	$S \cdot \nabla\boldsymbol{J}_e \cdot T$	$-h_{eff}(T - T_\infty)\frac{A}{V}$

The final expression of the governing equation of the model, as listed in equation (2), is obtained by substituting the source terms in Table 2 to equation (1) and neglecting the Bridgman effect, and simplifying the Peltier source as a boundary source.

$$\rho C_p \frac{\partial T}{\partial t} = \nabla(\kappa_{tot}\nabla T) + \frac{\boldsymbol{J}_e^2}{\sigma} - \tau\boldsymbol{J}_e \cdot \nabla T \tag{2}$$

The electric current is computed by the open-circuit voltage divided by the total resistance in the circuit, and the current density is the ratio of current to the cross-sectional area of the conductor, as shown in equation (3).

$$J_e = \frac{V_{emf}}{(R_{TE} + R_{load})A} \tag{3}$$

The open-circuit voltage generated by the Seebeck effect is determined by equation (4). S_h and S_c are total Seebeck coefficient of n-type and p-type materials and n is the number of TE couples.

$$V_{emf} = n(S_h T_h - S_c T_c) \tag{4}$$

The output voltage equals the open-circuit voltage generated by TE material subtracting the voltage drop due to the internal resistance of the TE material.

$$V = V_{emf} - IR_{TE} \tag{5}$$

The power generated by the TE circuit is calculated as

$$P = IV \tag{6}$$

2.2 Solutions to the Model

The domain of the TE leg is rectangular with a size of Lx·Ly·Lz in a three-dimensional cartesian coordinate system. The electric current flows along the z-direction. The first step to solve the PDE by a numerical iterative method is to discretize the domain into Nx·Ny·Nz identical-size cells and transform the physical equation into a discretized form by the FVM. The mesh generated for the TE element is shown in Figure 3. The control volume (CV) is one of the 3D

cells. The node, which determines the temperature profile of interest is in the center of the cuboid. A first-order explicit Euler scheme was adopted for the transient term of the governing equation in equation (2). The central difference scheme was adopted for the convection and diffusion terms in equation (2). As a result, the discretized governing equation can be written in equation (7).

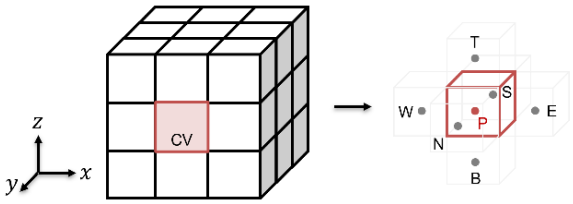

Figure 3: Schematic diagrams of the discretized domain and the control volume of a TE element.

$$\rho C_p \frac{T_P^{t+1} - T_P^t}{\Delta t} = \kappa_{tot}\left[\frac{T_W^t + T_E^t - 2T_P^t}{(\Delta x)^2} + \frac{T_S^t + T_N^t - 2T_P^t}{(\Delta y)^2} + \frac{T_B^t + T_T^t - 2T_P^t}{(\Delta z)^2}\right] + \frac{J_e^2}{\sigma} - \tau J_e \frac{T_T^t - T_B^t}{2\Delta z} \qquad (7)$$

The model algorithm is illustrated in Figure 4. The input parameters include material properties, geometry and sizes, number of discretized segments, time interval, and the initial and boundary conditions of temperature and voltage. The model calculated the temperature of interest in the next time step using temperature profiles at the current state. After iterations with respect to positions and time, the model checks output all temperature data and check the convergence of the result.

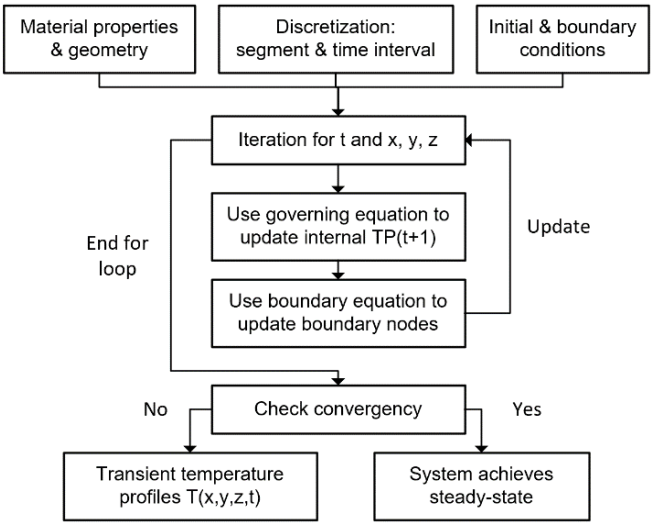

Figure 4: Flow chart of the model algorithm.

3. MODEL VALIDATION

3.1 Experimental Setup

The model was verified by the data obtained from the experiment. The experiment was carried out in Birck Nanotechnology Center (BNC) at Purdue University to test the performance of a commercially available TE module. The TE module is made of hundreds of TE couples, the soldering material, ceramic substrates, and wires. The experiment tested the power generation of the TE module given different temperature differences.

Figure 5 and **Figure 6** show the schematic diagram and digital photos of the experimental setup used for evaluating the thermal and electrical performance of a TE module, respectively. The setup consisted of four main parts including the TE module, the circulation units (i.e., water pipes, chillers, and valves), the micro-channel heat exchanger, and the measuring instrument (i.e., thermocouples, flow meters, multimeter, resistors, and data acquisition system). The

detailed specifications of the measurement device are listed in Table 3. In this study, the testing module was placed between two copper-made micro-channel heat exchangers with water flowing inside. The hot water from a heating recirculating chiller flowed into the upper heat exchanger and transfer heat flux to the TE module. The cold water from a cooling recirculating chiller flowed into the lower heat exchanger and remove heat flux from the TE module. Valves and flow meters were installed on the water pipe. Eight thermocouples (TC) are employed to measure temperatures of the selected locations, including the water inlets and outlets, the exterior surfaces of the TE module. The data from thermocouples was transferred and saved to a data logger. The multimeter was applied to measure the open-circuit voltage, as well as the closed-circuit voltage and current when connecting with different load resistors. The power output from the TE generator was calculated by equation (6).

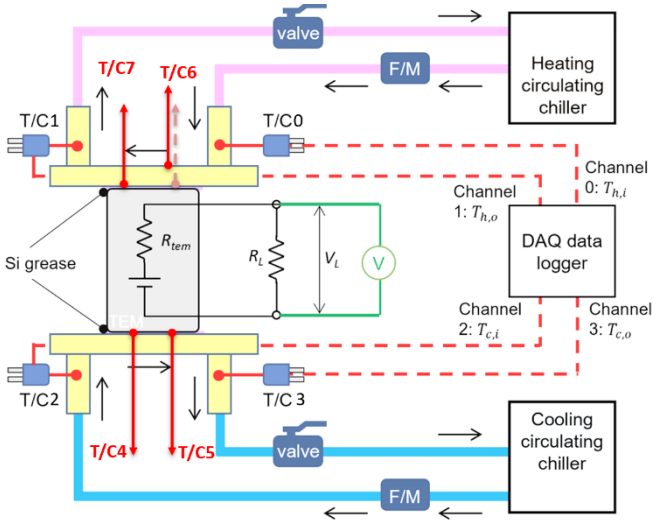

Figure 5: Schematic diagram of the test setup

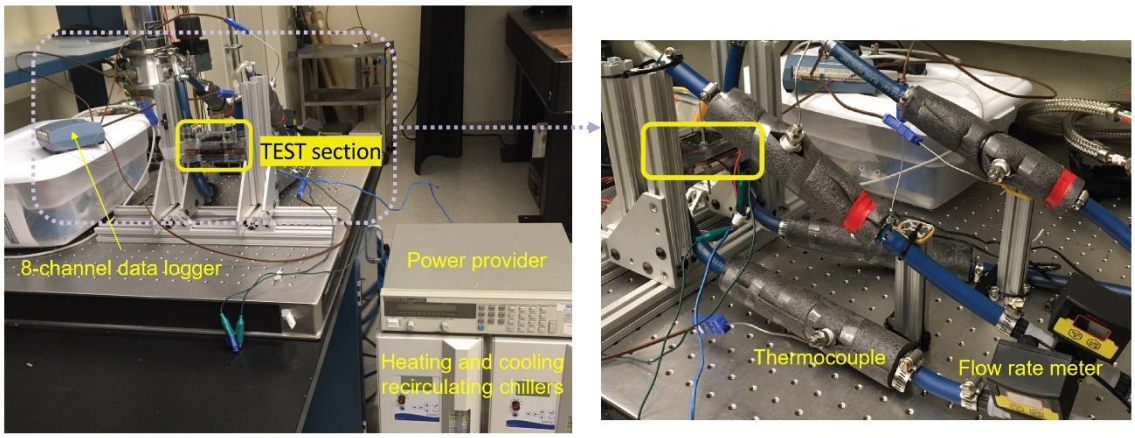

Figure 6: Digital photos of the test setup

Table 3: Parameters of the devices and instruments used in the test

Parameters/functions	Measurement devices	Sensitivity	Accuracies	Ranges
Temperature	T-type thermocouples	0.0001°C	> 1.0°C/0.75%	-250° to 350°C (-418° to 662°F)
Temperature	E-type thermocouples	0.0001°C	> 1.7°C/0.5%	-200° to 900°C (-328° to 1652°F)
Voltage	Fluke 189 multimeter	0.1mV, max 1 μV	± (0.025%+5)	0~1000V
Data logger	OM-USB-5201	0.0001°C	-	-

Chiller	Fisher Scientific Isotemp 250LCU	-	± 0.1°C	5~50°C (our test) -10~80°C (designed)
Flowmeter	Omega FTB 333D	0.01mL/min	± 6%	0.2~2L/min

3.2 Experimental Result and Comparison

The module was purchased from TE technology Inc with a series number of HP-199-1.4-0.88. The flow rates of both hot water and cold water were set at 150, 300, and 500 mL/min, approximately. The set-point temperature of the hot water was selected at 22 °C, 30 °C, 40 °C, and 50 °C, while the set-point temperature of the cold water was maintained at 7 °C. The voltage and current were measured when the system was steady. The TE transport properties of the commercial TE module are summarized in Table 4.

Table 4: Summary of values of the parameters used in the model

Classification	Parameters	Values	Units	Source
TE properties	Electrical conductivity	5917	S/m	Measured
	Thermal conductivity	1.6	W/m.K	Estimated
	Seebeck coefficient	208	μV/K	Datasheet
	Specific heat capacity	200	J/kgK	Estimated
	Density	7700	Kg/m^3	Estimated
Dimensions	Length of TE leg	0.88	mm	Datasheet
	Cross-sectional area of TE leg	1.4*1.4	mm^2	Datasheet
	Number of TE couples	199	-	Datasheet
Boundary conditions	Temperature of sink	280	K	Measured
	Temperature of source	313~323	K	Measured

The results of the Power-Resistance curve obtained from both experiment and model are compared and plotted in Figure 7. It can be observed that the higher the hot side temperature, the higher the temperature difference, and then the larger the voltage and power generated. From the comparison, we can find that the largest discrepancy between the experimental result and the modeling result is lower than 10%. There is a good agreement between the measurement data and the predicted data.

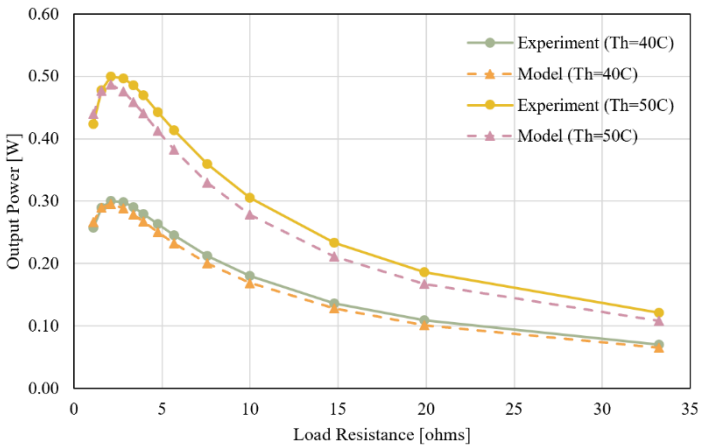

Figure 7: Comparison of power obtained from experiment and model with different load resistors

4. PERFORMANCE ANALYSIS

In this section, the performance of a TE module with cement composite based TE materials, are simulated. The TE transport properties of the TE cement composite were referred to (Ghosh et al., 2020), as listed in Table 5. The property of ceramic boards was obtained from (*Aluminum Nitride (AlN) Ceramic - Precision Ceramics USA*, n.d.). The property

of copper contact referred to (*ASM Handbook Volume 2: Properties and Selection: Nonferrous Alloys and Special-Purpose Materials - ASM International*, n.d.). The thermal contact resistance was also considered in the physical model and its value was referred to (Högblom & Andersson, 2014; Ouyang & Li, 2016). In this case, we consider the n-type and p-type TE cement shares the same TE properties while the only difference is the sign of the Seebeck coefficient. The modeling results are presented below.

Table 5: Summary of values of the parameters used in the baseline model

Classification	Parameters	Values	Units
Transport properties of TE material	Electrical conductivity	1390	S/m
	Thermal conductivity	0.99	W/m.K
	Seebeck coefficient	87E-6	V/K
	Specific heat capacity	0.63	J/gK
	Density	238	Kg/m^3
	Thermal contact resistance	1E-4	m^2K/W
Property of ceramic board	Thermal conductivity	180	W/m.K
Property of copper contact	Thermal conductivity	385	W/m.K
Dimensions of TE material	Length/ Thickness	1.5	cm
	Area	1.5×1.5	cm^2
	Number of TE couples	199	-
Dimensions of ceramic board/copper	Thickness	0.2	cm
Boundary and initial conditions	Convective heat transfer coefficient	10	W/m^2K

4.1 Power Generation Mode

In the summer, due to convection between hot air and the surface, as well as strong solar radiation, the external surface of the wall can almost reach 60 ºC, while the indoor air temperature is set at 22 ºC. In this situation, the air temperature difference is 40 ºC, and the output power density from the cementitious TEG module is about 0.3742 W/m^2, by assuming the fill factor is near 1. As shown in Figure 8, the cementitious TEG takes about 10 minutes to achieve the steady-state and the surface temperatures start to converge. Finally, the hot-side and cold-side interface temperatures become 315.09 ºC and 312.77 ºC, respectively.

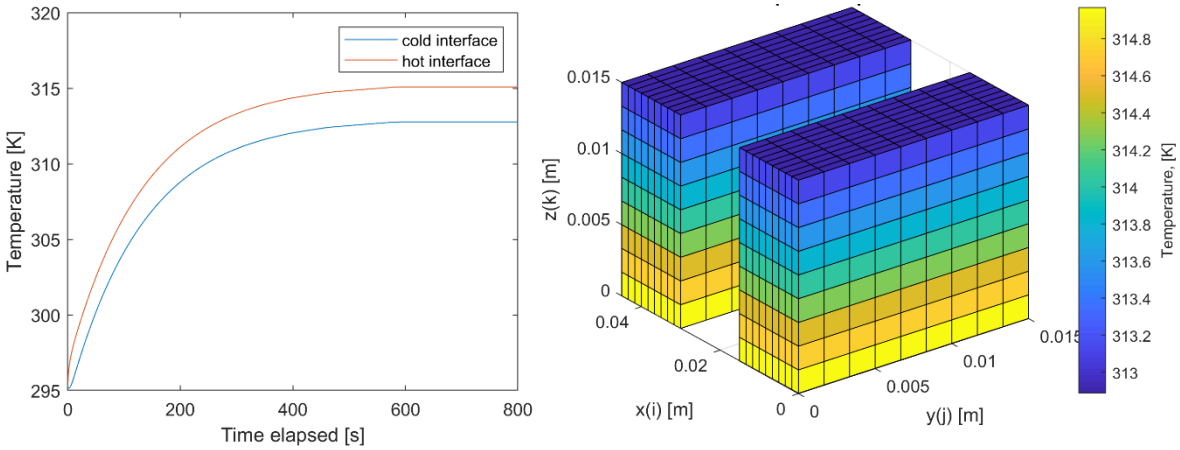

Figure 8: (a) The surface temperature of TEG with time elapsed and (b) the converged 3D temperature profile for TE legs.

4.2 Cooling Mode

In the cooling mode, both indoor and outdoor air temperatures and initial temperature are considered to be 25 ºC. When the power is input to the TE module, due to the Seebeck effect, the TE module can absorb heat at the cold side to achieve the purpose of cooling. As shown in Figure 9, with 10V voltage input, we observe that the cold side temperature first decreases and then increases over time. This is mainly due to excessive Joule heat and conductive heat. Cement-based materials have large resistance, therefore, will produce more joule heat, which will offset the

amount of cooling power. Besides, as the temperature on the hot side continues to rise, due to the Fourier heat conduction law, the energy on the hot side will be transported to the cold side in the form of heat conduction, affecting the cooling capacity.

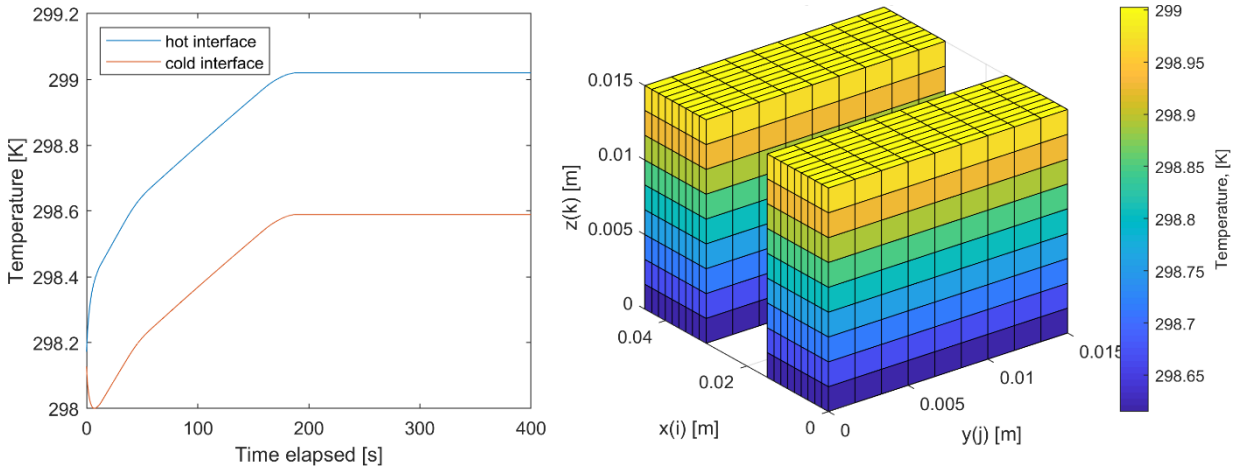

Figure 9: (a) The surface temperature of TEC with time elapsed and (b) the converged 3D temperature profile for TE legs.

5. CONCLUSIONS

In this study, a 3D transient heat and electric transport model was established for the thermoelectric module. The model was verified by the experimental test, and the discrepancy between the modeling results and the experimental data was less than 10%. Then, the model was used to simulate the performance of the cement-based thermoelectric module. The results showed that, in the power generation mode, the cement-based thermoelectric module can achieve a power density around 0.37 W/m^2. In the cooling mode, due to the large resistance of the material and a low figure of merit (ZT), the cold side cannot be effectively cooled. Therefore, it is necessary to find better cement-based thermoelectric materials with higher ZT and smaller electrical resistance to realize more efficient cooling. Besides, the model has high computational efficiency. In the future, the model will be used for the simulation of TE modules in building systems.

NOMENCLATURE

FDM	Finite difference method	(–)
FEM	Finite element method	(–)
FVM	Finite volume method	(–)
PDE	Partial differential equation	(–)
TE	Thermoelectric	(–)
TEC	Thermoelectric cooler	(–)
TEG	Thermoelectric generator	(–)
TEM	Thermoelectric module	(–)
ZT	Figure of merit coefficient	(–)

REFERENCES

Aluminum Nitride (AlN) Ceramic - Precision Ceramics USA. (n.d.). Retrieved January 29, 2021, from https://precision-ceramics.com/materials/aluminum-nitride/

Antonova, E. E., & Looman, D. C. (2005). Finite elements for thermoelectric device analysis in ANSYS. *ICT 2005. 24th International Conference on Thermoelectrics, 2005.*, 215–218. https://doi.org/10.1109/ICT.2005.1519922

ASM Handbook Volume 2: Properties and Selection: Nonferrous Alloys and Special-Purpose Materials - ASM

International. (n.d.). Retrieved January 29, 2021, from https://www.asminternational.org/search/-/journal_content/56/10192/06182G/PUBLICATION

El-Genk', M., Saber', H., & Caillat2, T. (2004). *HIGH EFFICIENCY THERMOELECTRIC RADIOISOTOPE POWER SYSTEMS Final Report*. https://ntrs.nasa.gov/search.jsp?R=20040084240

Fateh, H., Baker, C. A., Hall, M. J., & Shi, L. (2014). High fidelity finite difference model for exploring multi-parameter thermoelectric generator design space. *Applied Energy*, *129*, 373–383. https://doi.org/10.1016/j.apenergy.2014.04.088

Ghosh, S., Harish, S., Ohtaki, M., & Saha, B. B. (2020). Enhanced figure of merit of cement composites with graphene and ZnO nanoinclusions for efficient energy harvesting in buildings. *Energy*, *198*, 117396. https://doi.org/10.1016/j.energy.2020.117396

Ghosh, S., Harish, S., Rocky, K. A., Ohtaki, M., & Saha, B. B. (2019). Graphene enhanced thermoelectric properties of cement based composites for building energy harvesting. *Energy and Buildings*, 109419. https://doi.org/10.1016/j.enbuild.2019.109419

Goupil, C. (n.d.). *Continuum theory and modeling of thermoelectric elements*.

Hogan, T. P., & Shih, T. (2005). Modeling and characterization of power generation modules based on bulk materials. In D. M. Rowe (Ed.), *Thermoelectrics Handbook: Micro to Nano*. CRC Press.

Högblom, O., & Andersson, R. (2014). Analysis of thermoelectric generator performance by use of simulations and experiments. *Journal of Electronic Materials*, *43*(6), 2247–2254. https://doi.org/10.1007/s11664-014-3020-x

IEA (2020). (n.d.). *Tracking Buildings 2020 – Analysis - IEA*. Retrieved January 11, 2021, from https://www.iea.org/reports/tracking-buildings-2020

Jang, J. Y., & Tsai, Y. C. (2013). Optimization of thermoelectric generator module spacing and spreader thickness used in a waste heat recovery system. *Applied Thermal Engineering*, *51*(1–2), 677–689. https://doi.org/10.1016/j.applthermaleng.2012.10.024

Liu, X., Jani, R., Orisakwe, E., Johnston, C., Chudzinski, P., Qu, M., Norton, B., Holmes, N., Kohanoff, J., Stella, L., Yin, H., & Yazawa, K. (2020). State of the art in composition, fabrication, characterization, and modeling methods of cement-based thermoelectric materials for low-temperature applications. In *Renewable and Sustainable Energy Reviews* (Vol. 137, p. 110361). Elsevier Ltd. https://doi.org/10.1016/j.rser.2020.110361

Nguyen, N. Q., & Pochiraju, K. V. (2013). Behavior of thermoelectric generators exposed to transient heat sources. *Applied Thermal Engineering*, *51*(1–2), 1–9. https://doi.org/10.1016/j.applthermaleng.2012.08.050

Oliveira, K. S. M., Cardoso, R. P., & Hermes, C. J. L. (2014). Two-Dimensional Modeling of Thermoelectric Cells. *International Refrigeration and Air Conditioning Conference*. https://docs.lib.purdue.edu/iracc/1357

Ouyang, Z., & Li, D. (2016). Modelling of segmented high-performance thermoelectric generators with effects of thermal radiation, electrical and thermal contact resistances. *Scientific Reports*, *6*(1), 1–12. https://doi.org/10.1038/srep24123

Pfeiffelmann, B., Benim, A. C., & Joos, F. (2018). A Finite Volume Analysis of Thermoelectric Generators. *Heat Transfer Engineering*, 1–9. https://doi.org/10.1080/01457632.2018.1474588

Rodríguez, A., Vián, J. G., Astrain, D., & Martínez, A. (2009). Study of thermoelectric systems applied to electric power generation. *Energy Conversion and Management*, *50*(5), 1236–1243. https://doi.org/10.1016/j.enconman.2009.01.036

Svobodová, S., & Matějka, L. (2014). Maximum Temperatures Of Roof Tiles During The Summer Period. *Advanced Materials Research*, *1041*, 303–306. https://doi.org/10.4028/www.scientific.net/AMR.1041.303

Yan, D., Dawson, F. P., Pugh, M., & El-Deib, A. A. (2014). Time-dependent finite-volume model of thermoelectric devices. *IEEE Transactions on Industry Applications*, *50*(1), 600–608. https://doi.org/10.1109/TIA.2013.2271272

Zuazua-Ros, A., Martín-Gómez, C., Ibañez-Puy, E., Vidaurre-Arbizu, M., & Gelbstein, Y. (2019). Investigation of the thermoelectric potential for heating, cooling and ventilation in buildings: Characterization options and applications. *Renewable Energy*, *131*, 229–239. https://doi.org/10.1016/J.RENENE.2018.07.027

ACKNOWLEDGEMENT

This paper is based upon work supported by the National Science Foundation under grant no. CBET-1805818.